Multiple phase separation of super-abundant-vacancies in Pd hydrides by all solid-state electrolysis in moderate temperatures around 300°C

Yoshiki Fukada[a,*], Tatsumi Hioki[b], Tomoyoshi Motohiro[b]

[a] *Toyota Motor Corporation, 1200 Mishuku, Susono-shi, Shizuoka-ken, 410-1193, Japan*
[b] *Green Mobility Collaborative Research Center & Graduate School of Engineering Nagoya University, Furo-cho, Chikusa-ku, Nagoya 464-8603, Japan*

Abstract

The dynamics of hydrogen-induced vacancies are the key for understanding various phenomena in metal–hydrogen systems under a high hydrogen chemical potential. In this study, a novel dry-electrolysis experiment was performed in which a hydrogen isotope was injected into a Pd cathode and time-resolved *in situ* monochromatic X-ray diffraction measurement was carried out at the Pd cathode. It was found that palladium-hydride containing vacancies forms multiple phases depending on the hydrogen chemical potential. Phase separation into vacancy-rich, vacancy-poor, and moderate-vacancy-concentration phases was observed when the input voltage was relatively low, i.e., ~ 0.5 V. The moderate-vacancy-concentration phase may be attributed to Ca_7Ge or another type of super-lattice $Pd_7VacH(D)_8$. Transition from the vacancy-rich to the moderate-vacancy-concentration phase explains the sub-micron void formations without high temperature treat-

*Corresponding author
Email address: yoshiki_fukada@mail.toyota.co.jp (Yoshiki Fukada)

ment that were observed at the Pd cathode but have never been reported in previous anvil experiments.

Keywords: metal hydrides, solid-electrolyte, electrical transport, hydrogen-induced-vacancies, X-ray diffraction, electrolysis

1. Introduction

The use of hydrogen in industrial applications is increasing because of growing demand for clean energy. Knowledge about the interactions between hydrogen and metals is of fundamental importance to facilitate this use.

One prominent recent discovery concerning this metal–hydrogen interaction is the formation of super-abundant-vacancies. Fukai *et al.* loaded hydrogen into metals at high pressures between 3 and 5 GPa and high temperatures between 600 and 900°C using an anvil technique. The lattice contractions of the metal-hydrides observed by Fukai *et al.* were attributed to the formation of hydrogen-induced super-abundant-vacancies[1–3]. Super-abundant-vacancies play a crucial role in metal–hydrogen systems. It has been reported that a major cause of hydrogen embrittlement is crack growth by agglomerations of vacancies[4–6]. Other research found that these vacancy formations significantly affect electrodeposited metals[7–9] via extremely enhanced diffusion[10–12]. This phenomenon may even be applicable for industrial use.

It was pointed out that the trapping of hydrogen atoms in a vacancy assists vacancy formation[13–16]. The trapping of hydrogen atoms by a metal atom vacancy lowers the vacancy formation energy, which is replaced with the formation energy of a vacancy–hydrogen cluster. For theoretical veri-

fication, Fukai, Harada and Sugimoto conducted a Monte Carlo simulation of vacancy formation in metal-hydrides[17, 18], which demonstrated that the vacancy–hydrogen binding energy significantly affects the vacancy concentration. In the simulation, phase separation into vacancy-rich and vacancy-poor phases, which is due to a long-range elastic interaction between vacancies, was observed.

Several theoretical studies have been made into the phase diagrams of metal-hydrides containing vacancies. Zhang and Ali Alavi evaluated the vacancy formation energy in metals using a density-functional theory[19], and showed that a Pd_3VacH_4 structure is stable with lattice parameters close to the bulk Pd. Yu *et al.* studied the stability of vacancies in metal-hydrides using a thermodynamic theory[20], and found that a vacancy-ordered $L1_2$ structure phase and a vacancy-poor A1 structure phase co-exist in a specific range of temperatures and hydrogen concentrations. Nazarov *et al.* successfully demonstrated the phase changes of metals into metal-hydrides or vacancy-ordered hydride phases in high hydrogen chemical potentials in an *ab initio* calculation[21], and pointed out that a high hydrogen chemical potential lowers the formation energy of a vacancy–hydrogen cluster. This is a key to understanding vacancy formation under high hydrogen chemical potentials.

The generation of high hydrogen chemical potentials is one key for experimental studies. Water electrolysis has been used for many such studies[22–24] as well as a plasma-injection technique[25, 26]. We developed a novel dry-electrolysis method using a solid-state electrolyte to load a hydrogen isotope into metal cathodes[27]. The advantage of this method is that the input

voltage directly reflects the hydrogen chemical potential due to the capacitor-like configuration and the solid-state sealing on the cathode. Experiments using this method have observed remarkable formations of super-abundant-vacancies and phase separation into vacancy-rich and vacancy-poor phases.

Some differences have occurred between the results of the anvil experiments mentioned above and the dry-electrolysis experiments. According to the thermodynamic theory and anvil experiments, Fukai *et al.*[16] found that the maximum vacancy concentration limit in Pd : x_{vmax} =Vac/Pd is 0.163. In contrast, the results of dry-electrolysis experiments attained a vacancy concentration of $x_{vmax} = 0.33$. Moreover, these experiments also revealed the existence of numerous sub-micron scale voids in the recovered samples, which were attributed to the agglomeration of vacancies. Although sub-micron scale voids were also found in Ni[28] and Pd[29, 30] in the anvil experiments, high temperature treatments were required to form these voids. The differences between the anvil and dry-electrolysis experiments seem to be attributable to the difference in the chemical potential of hydrogen. However, a consistent understanding about the different results obtained by the anvil and dry-electrolysis experiments has not been established.

The aim of the work described in this paper is to explore the region between the high hydrogen chemical potential formed by the anvil experiments and the extremely high chemical potential formed by dry-electrolysis. In this study, dry-electrolysis was performed with a comparatively low input voltage. A remarkable multiple phase separation attributable to different vacancy concentration phases was observed. The crystal structures and vacancy formation energies of these phases will also be discussed below.

2. Experimental method

An electrolysis reactor consisting of a Cr intermediate layer, a Pd cathode layer, a solid-state electrolyte layer, an outermost Pd anode layer, and Au contact electrodes was deposited on a SiO_2 substrate by sputtering. A perovskite-type compound $BaZr_{1-x}Y_xO_3$ with $x \simeq 0.2$ was used for the solid-state electrolyte. Figure 1 shows the stack structure of the solid state electrolysis reactor. The sputtering conditions of the solid state electrolyte depositions are on Table 1. In previous experiments, Rh was mixed into the Pd cathode to make the crystal grains finer and to obtain smooth diffraction lines. In this experiment, Rh was not used and the crystal grains were coarser. This resulted in granular diffraction lines consisting of clusters of many spots. It is unknown how coarser crystal grains affect vacancy formation.

The reactor was placed in a chamber equipped with electrodes, a heater to control the reactor temperature, and X-ray windows. The chamber was filled with 0.013 MPa of hydrogen isotope gas mixed with the same molar amount of nitrogen. Deuterium was chosen for the hydrogen isotope because it shows faster vacancy formation than hydrogen, which was favourable for the purpose of this experiment.

The mechanism of hydrogen isotope loading is the electric transfer of protons/deuterons into the metal cathode via solid-state electrolytes. Deuterium was supplied from a gas phase atmosphere in the chamber via the Pd anode. The input voltage V applied between the anode and the cathode controls the chemical potential of deuterium on the cathode μ_{D2}.

$$\mu_{D2} - \mu_{D2}^{cham} = 2eV \tag{1}$$

where, μ_{D2}^{cham} is the chemical potential of deuterium in the chamber atmosphere.

In situ monochromatic X-ray diffraction measurements were carried out in beam line BL5S2 at the Aichi Synchrotron Radiation Center of the Aichi Science & Technology Foundation. The X-ray wavelength was set to 0.07 nm, which corresponds to an X-ray energy of 17.713 keV. The incident angle of the X-ray to the reactor was fixed to 10 degrees. The diffracted X-rays were detected by a Rigaku Pilatus 100K pixel detector and Fujifilm BAS-MS 2040 imaging plate.

More details about the experimental method can be found in our previous paper[27].

3. Results and discussion

3.1. In situ X-ray diffraction measurements

Figure 2 shows the input voltage, the current and the temperature as a function of time. Figure 3 shows the diffraction patterns obtained by the pixel detector. Diffraction images taken by the imaging plate are shown in Figure 4. The observed diffraction lines—denoted as 111, 200, and 220—are from the Pd cathode. A high initial input voltage of 6 V was applied for a period of 22 minutes after the temperature reached 200°C. This process is called the "reduction process" to reinforce the adhesion between the electrolyte and the Pd cathode.

After the reduction process, the input voltage was lowered to 2 V. The diffraction lines from the Pd cathode rapidly shifted to lower angles with time. This is the result of a large increase in the lattice parameter, which

indicates the amount of loaded deuterium. These diffraction lines from the Pd cathode are labelled as A or A111 (phase A) in the figure. The phase separations after 63 to 67 minutes are ordinal spinodal decompositions into deuterium-rich and deuterium-poor phases.

After 70 minutes, a phase with a small lattice parameter close to the bulk Pd appeared. This phase is called phase B, which seems to be same phase observed in the previous experiments[27]. According to the discussion in that experiment, and the large lattice contraction rate, phase B can be judged to be a vacancy-rich phase.

After 95 minutes, the input voltage was further lowered to 0.5 V to observe the reaction under a low input voltage. Subsequently, the diffraction images showed quite complex patterns. A new phase with a slightly smaller lattice parameter than phase A appeared—called phase C. In the time range from 102 to 123 minutes, phase A, phase B, and phase C co-existed and the diffraction patterns are nearly unchanged for that period. Figure 5 shows an angle distribution of the diffraction obtained from the imaging plate after 110 minutes. The diffraction lines C111 and C200 can be recognized as small sub-peaks near phase A.

After 145 minutes, the input voltage was increased to more than 2 V. As a result, phase A disappeared and the diffraction lines of phase C seemed to shift to higher angles. After 175 minutes, only phase B can be seen. After $\sim$ 140 minutes, the current dropped, possibly indicating that the chemical potential of deuterium rose up to the level of the input voltage. It should be noted that diffraction lines from the electrolyte appeared after 152 minutes, possibly due to re-crystallization of the initially amorphous electrolyte

through an annealing effect during the electrolysis.

3.2. Lattice parameters

The lattice parameters were evaluated by X-ray diffraction. The lattice parameters were compared with a model. Linear dependences between lattice parameter a and vacancy-concentration x_v =Vac/Pd and hydrogen concentration x_h =H(D)/Pd are assumed.

$$a = a_o(1 + \alpha_h x_h - \alpha_v x_v) \tag{2}$$

where, a_o is the lattice parameter of defect-free pure Pd, α_h is the lattice expansion coefficient due to hydrogen absorption, and α_v is the lattice contraction coefficient due to vacancy formation. This model ignores the heat expansion since it is relatively small. According to known hydrogen partial pressures for various temperatures[36], the spinodal decomposition in the beginning of the experiment can be assumed to be $PdD_{0.2}$ and $PdD_{0.5}$, which correspond to either end of the flat region in in the hydrogen content–hydrogen partial pressure relationship. The lattice constant of Pd_3VacH_4 is expected to be close to that of pure Pd[19]. From this information, the parameters can be assumed to be as follows: $\alpha_h = 0.07$ and $\alpha_v = 0.27$. Phases B and C show good agreement with Pd_3VacD_4 and Pd_7VacD_8 respectively. Figure 6 compares the estimated lattice parameters and the measured values. It is notable that phase A contains quite a large amount of vacancies, which may be due to the slow deuterium injection. It is known that hydrogen atoms enter a metal lattice along with vacancies when the hydrogen chemical potential is high[14].

3.3. Electron microscopy observation of Pd cathodes

After the experiment, the reactor was observed using a scanning transmission electron microscope (STEM). The sample was prepared by FIB. Figure 7 shows the STEM images. In the STEM images, numerous sub-micron scale voids can be seen. Similar sub-micron voids were observed in our previous experiments as reported earlier[27]. Dendrite-like Pd precipitates were also observed but the amount of precipitate is less than previously observed. Although some discussions have been made concerning the formation of these precipitates[27], the cause is still unknown. Enhanced atomic migration of Pd from the cathode associated with the vacancy formation is the most possible cause of the precipitate.

As described above, slight diffraction lines from the electrolyte were observed. This is different from the results of previous experiments. The reproducibility of electrolyte fabrication is poor and the reactor electrolyte quality—i.e., the crystallinity and the density—in this experiment seemed to be higher than in the previous experiments. This relatively high electrolyte quality may result in lower leak current and less formation of dendrite-like Pd precipitates.

3.4. Modelling

3.4.1. Vacancy–hydrogen binding energy and crystal structure

It is known that the position of trapped hydrogen atoms shifts toward a vacancy from their original interstitial site[31]. Following discussions considers a case in which a vacancy exists in a PdH lattice and another vacancy is introduced in the vicinity of the first vacancy. If the new vacancy is positioned at [110], [101], or [011]—an opposite corner on the diagonal line of the

cube face (fourth-neighbour O-site), it may have little effect on the binding energy between the vacancy and the hydrogen atoms. In contrast, if the new vacancy is positioned at [100], [010], or [001]—an adjoining corner of the cubic structure (second-neighbour O-site), a hydrogen atom will be positioned between the two vacancies. The position of the hydrogen atom will move back to the centre between the vacancies—i.e., the distance between the hydrogen atom and vacancies increases. As the result, the binding energy decreases.

From this discussion, it can be interpreted that weak short-range repulsive interaction exists between vacancies at second-neighbour O-sites. It should be noted that a fairly high formation energy for a pair of vacancies at nearest-neighbour O-sites (the adjoining face centres from the cube corner) has been reported[32]. This means that there is a strong repulsive interaction between vacancies at nearest-neighbour O-sites which inhibits the formation of vacancies at these sites. Consequently, the composition of the maximum vacancy concentration without reduction of the binding energies was found to be $Pd_7VacH_{6\sim8}$. This phase is called the moderate-vacancy-concentration phase, which may have appeared as phase C in the experiment results described above.

As shown in Figure 8, the crystal structure is a Ca_7Ge type super-lattice. A similar lattice structure has also been reported in an Mg_6VH_x hydrogen storage alloy[33]. Super-lattice reflections that break the fcc extinction rule were reported in several experiments[2, 34]. Super-lattice reflections were not observed in our dry-electrolysis experiments, possibly because the long distance orders were not sufficiently established at the considerably lower

temperature range and shorter duration.

Since vacancy formation at third-neighbour O-sites—the face centre at the opposite side from a cube corner—is also possible, there is another possible crystal structure for $Pd_7VacH_{6\sim8}$. Figure 9 shows the crystal structure. The actual structure is unknown—it strongly depends on vacancy–vacancy interaction. Ab initio calculations may be a good means to examine realistic structures.

Metal-hydrides are good examples of super-lattice structures. It is known that metal-hydrides have quite complex phase-diagrams in the low temperature region[35, 36]. Those phases are attributed to super-lattice structures due to short-range hydrogen–hydrogen interactions[37]. Hence, there is a possibility that vacancy-ordered super structures also exhibit complex phase diagrams due to the short-range vacancy–vacancy interactions in lower temperature regions similar to that in hydrogen-ordered super structures in metal-hydrides.

3.4.2. Vacancy concentration

The limit concentration of $x_{vmax} = 0.163$ determined by Fukai *et al.*[16] is close to the vacancy concentration of $Pd_7VacH_{6\sim8}$ ($x_v = 1/7 \simeq 0.143$). According to the Monte Carlo simulation study[17], the vacancy concentration is very sensitive to the vacancy–hydrogen binding energy. A small change in the binding energy—less than 0.1 eV—induces a huge change in the vacancy concentration. As shown above, introduction of an additional vacancy into the $Pd_7VacH(D)_x$ lattice may cause a reduction in binding energy. Hence, increases in vacancy concentration beyond $Pd_7VacH(D)_x$ are virtually inhibited. This is a reasonable explanation for the limit concentration determined

by Fukai *et al.*. However, dry-electrolysis experiments may break this limit due to the extremely high hydrogen/deuterium chemical potential, forming vacancy-rich phases $Pd_3VacH(D)_4$.

From Equation (1) and known chemical potentials for hydrogen in various conditions[36], equivalent hydrogen pressures at the cathode are obtained as shown in Table 2. To obtain the values in Table 2, the following formula was used to obtain a smooth extrapolation between the given discrete values of the pressures and the chemical potentials.

$$\sqrt{p} - \sqrt{p_0} = C_1(\mu_H - \mu_H^0) + C_2(T - T_0) \tag{3}$$

where, p is the pressure, μ_H is the hydrogen chemical potential, T is the temperature and C_1 and C_2 are constants. Although the values for deuterium are unknown, these should be close to the values for hydrogen. The equivalent hydrogen pressure for 1.0 V of input voltage is 15.9 GPa. This is far above the condition in the anvil experiments. At such a high hydrogen/deuterium chemical potential, only the vacancy-rich phase may be stable. In contrast, the equivalent hydrogen pressure under 0.5 V of input voltage is 3.22 GPa. This condition is close to the one in the anvil experiments.

Nazarov *et al.* pointed out that the Gibbs formation energy of a hydrogen–vacancy cluster containing n_H hydrogen atoms under a high hydrogen chemical potential G_f^δ is the sum of the formation energy of a hydrogen–vacancy cluster $G_f^{\delta,0}$ and an energy to take n_H hydrogen atoms out from their chemical reservoir μ_H[21].

$$G_f^\delta = G_f^{\delta,0} - n_H(\mu_H - \mu_H^0) \tag{4}$$

where μ_H^0 is a reference chemical potential. When the formation energy of a hydrogen–vacancy cluster becomes zero, any number of vacancies can form.

As a result, multiple phases may co-exist. The vacancy–hydrogen cluster formation energy under a low hydrogen chemical potential is known to be 0.72 eV[16]. The present experiment result—multiple phases co-existing with an input voltage of around 0.5 V—is fairly consistent with these theoretical considerations.

3.4.3. Formation of voids

Sub-micron scale voids were found at the Pd cathodes of recovered reactors, possibly caused by agglomerations of vacancies[28]. If the vacancy–hydrogen clusters decompose, vacancies are no longer stable because of the loss of hydrogen. Agglomerations of vacancies may occur as a result[38]. In anvil experiments[28–30], high temperature treatment up to 800°C was needed to form these voids. Because of the strong trapping of hydrogen, the vacancy–hydrogen clusters remain stable even at elevated temperatures[39]. Hence, the moderate-vacancy-concentration phase $Pd_7VacH(D)_x$ may be still quasi-stable at moderate temperatures. However, the vacancy-rich phase $Pd_3VacH(D)_x$—which forms only with dry-electrolysis—may be stable only under a high chemical potential of hydrogen isotope. Transition from the vacancy-rich to moderate-vacancy-concentration phase may occur when the samples are returned to ambient conditions. The excess vacancies agglomerate and form voids.

4. Conclusions

Deuterium was loaded into Pd using the dry-electrolysis technique. Multiple phases were observed when the input voltage was lowered to 0.5 V,

which were attributed to vacancy-poor, vacancy-rich, and moderate-vacancy-concentration phases. When the input voltage is high, only a vacancy-rich phase forms. After considering the short-range vacancy–vacancy interaction due to multiple binding between hydrogen atoms and vacancies, a hypothesis was deduced in which the moderate-vacancy-concentration phase $Pd_7VacH(D)_8$ forms in a certain hydrogen chemical potential range. When the hydrogen chemical potential is very high—only attainable using the dry-electrolysis technique—the vacancy-rich phase $Pd_3VacH(D)_4$ forms. This model provides a consistent explanation for the results of anvil experiments and dry-electrolysis experiments. Transition from the vacancy-rich to the moderate-vacancy-concentration phase explains the void formation without high temperature treatment. This hypothesis—in which metal-hydrides containing vacancies change phase depending on the hydrogen chemical potential due to the short-range vacancy interactions—suggests the existence of more complex phase diagrams for metal-hydrides containing vacancies in lower temperature regions. The developed dry-electrolysis method is an effective tool for examining this field.

Issues for the future include further studies under different temperature and voltage conditions and different host metals—Ni, Cr, Co, Fe and Nb—as well as a theoretical examination of the thermo-dynamics of metal-hydrogen containing vacancies.

Acknowledgements

The authors would like to extend their gratitude to S.Umemura the former General Manager of the Future Project Division at Toyota Motor Corpora-

tion for his strong encouragement of our hydrogen–metal interaction study program. The *in situ* diffraction measurements were performed with the valuable assistance of H.Azuma, M.Yoshimura, Y.Nakanishi, M.Nouchi, and A.Wada at the Aichi Synchrotron Radiation Center of the Aichi Science & Technology Foundation. The precise STEM observation was carried out by T.Sugimoto at the Aichi Center for Industry and Science Technology.

References

[1] Y. Fukai, N. Ōkuma, Evidence of Copious Vacancy Formation in Ni and Pd under a High Hydrogen Pressure, Jpn.J.Appl.Phys., **32** (1993) L1256–L1259.

[2] Y. Fukai, N.Ōkuma, Formation of Superabundant Vacancies in Pd Hydride under High Hydrogen Pressures, Phys.Rev.Lett., **73** (1994) 1640.

[3] S. Harada, S. Yokota, Y. Ishii, Y. Shizuku, M. Kanazawa, Y. Fukai, A relation between the vacancy concentration and hydrogen concentration in the Ni–H, Co–H and Pd–H systems, J. Alloys Compd., **404–406** (2005) 247–251.

[4] Y. Tateyama and T. Ohno, Stability and clusterization of hydrogen–vacancy complexes in α-Fe: An ab initio study, Phys. Rev., **B67** (2003) 174105.

[5] M. Nagumo, M. Nakamura, K. Takai, Hydrogen thermal desorption relevant to delayed-fracture susceptibility of high-strength steels, Metal.Mater.Trans. A, **32A** (2001) 339–347.

[6] M. Nagumo, Hydrogen related failure of steels—a new aspect, Mater.Sci.Tech., **20** (2004) 940–950.

[7] Y. Fukai, M. Mizutani, S. Yokota, M. Kanazawa, Y. Miura, T. Watanabe, Superabundant vacancy–hydrogen clusters in electrodeposited Ni and Cu, J. Alloys Compd., **356–357** (2003) 270–273.

[8] N. Fukumuro, T. Adachi, S. Yae, H. Matsuda, Y. Fukai, Influence of hydrogen on room temperature recrystallisation of electrodeposited Cu films: thermal desorption spectroscopy, Trans. Inst. Met. Finish., **89** (2011) 198–201.

[9] N. Hisanaga, N. Fukumuro, S. Yae, H. Matsuda, Hydrogen in Platinum Films Electrodeposited from Dinitrosulfatoplatinate(Ⅱ) Solution, ECS Trans., **50**(48) (2013) 77–82.

[10] K. Watanabe, N. Ōkuma, Y. Fukai, Y. Sakamoto and Y. Hayashi, Superabundant vacancies and enhanced diffusion in Pd–Rh alloys under high hydrogen pressures, Scripta Materialia, **34**(4) (1996) 551–557.

[11] E. Hayashi Y. Kurokawa and Y. Fukai, Hydrogen-Induced Enhancement of Interdiffusion in Cu–Ni Diffusion Couples, Phys.Rev.Lett., **80**(25) (1998) 5588.

[12] N. Fukumuro, M. Yokota, S. Yae, H. Matsuda, Y.Fukai, Hydrogen-induced enhancement of atomic diffusion in electrodeposited Pd films, J. Alloys Compd., **580** (2013) s55–s57.

[13] Y. Fukai, Formation of superabundant vacancies in metal hydrides at high temperatures, J. Alloys Compd., **231** (1995) 35–40.

[14] Y. Fukai, Y. Kurokawa, H. Hiraoka, Superabundant Vacancy Formation and Its Consequences in Metal–Hydrogen Alloys, J. Japan Inst. Metals, **61** (1997) 663–670 (in Japanese).

[15] Y. Fukai, Y. Shizuku, Y. Kurokawa, Superabundant vacancy formation in Ni–H alloys, J. Alloys Compd., **329** (2001) 195–201.

[16] Y. Fukai, Y. Ishii, Y. Goto, K. Watanabe, Formation of superabundant vacancies in Pd–H alloys, J. Alloys Compd., **313** (2000) 121–132.

[17] Y. Fukai, H. Sugimoto, Formation mechanism of defect metal hydrides containing superabundant vacancies, J. Phys.: Condens. Matter, **19** (2007) 436201.

[18] Y. Fukai, H. Sugimoto, The defect structure with superabundant vacancies to be formed from fcc binary metal hydrides: Experiments and simulations, J. Alloys Compd., **446–447** (2007) 474–478.

[19] C. Zhang, Ali Alavi, First-Principles Study of Superabundant Vacancy Formation in Metal Hydrides, J. Am. Chem. Soc., **127**(27) (2005) 9808–9817.

[20] S.Yu. Zaginaichenko, Z.A. Matysina, D.V. Schur, L.O. Teslenko, A. Veziroglu, The structural vacancies in palladium hydride. Phase diagram, Int. J. Hydrogen Energy, **36** (2011) 1152–1158.

[21] R. Nazarov, T. Hickel, and J. Neugebauer, Ab initio study of H–vacancy interactions in fcc metals: Implications for the formation of superabundant vacancies, Phys. Rev. **B89** (2014) 144108.

[22] R. Felici, L. Bertalot, A. DeNinno, A. LaBarbera and V. Violante, In situ measurement of the deuterium (hydrogen) charging of a palladium electrode during electrolysis by energy dispersive x-ray diffraction, Rev. Sci. Instrum., **66**(5) (1995) 3344.

[23] E.F. Skelton, P.L. Hagans, S.B. Qadri, D.D. Dominguez, A.C. Ehrlich and J.Z. Hu, In situ monitoring of crystallographic changes in Pd induced by diffusion of D, Phys. Rev., **B58** (1998) 14775.

[24] D.L. Knies, V.Violante, K.S. Grabowski, J.Z. Hu, D.D. Dominguez, J.H. He, S.B. Qadri and G.K. Hubler, In-situ synchrotron energy-dispersive x-ray diffraction study of thin Pd foils with Pd:D and Pd:H concentrations up to 1:1, J. Appl. Phys., **112** (2012) 083510.

[25] C.E. Buckley, H.K. Birnbaum, D. Bellmann, P. Staron, Calculation of the radial distribution function of bubbles in the aluminum hydrogen system, J. Alloys Compd., **293–295** (1999) 231–236.

[26] H. Wulff, M. Quaas, H. Deutsch, H. Ahrens, M. Fröhlichc, C.A. Helm, Formation of palladium hydrides in low temperature Ar/H^2-plasma, Thin Solid Films, **596** (2015) 185–189.

[27] Y. Fukada, T. Hioki, T. Motohiro, S. Ohshima, In situ x-ray diffraction study of crystal structure of Pd during hydrogen isotope loading by solid-state electrolysis at moderate temperatures 250–300°, J. Alloys Compd., **647** (2015) 221–230.

[28] H. Osono, T. Kino, Y. Kurokawa, Y. Fukai, Agglomeration of hydrogen-induced vacancies in nickel, J. Alloys Compd., **231** (1995) 41–45.

[29] D.S dos Santos, S. Miraglia, D. Fruchart, A high pressure investigation of Pd and the Pd–H system, J. Alloys Compd., **291** (1999) L1–L5.

[30] D. S. dos Santos, S. S. M. Tavares, S. Miraglia, D. Fruchart, D. R. dos Santos, Analysis of the nanopores produced in nickel and palladium by high hydrogen pressure, J. Alloys Compd., **356–357** (2003) 258–262.

[31] O.Yu. Vekilova, D.I. Bazhanov, S.I. Simak, I.A. Abrikosov, First-principles study of vacancy–hydrogen interaction in Pd, Phys.Rev., **B80** (2009) 024101.

[32] I.A. Supryadkina, D.I. Bazhanov, and A.S. Ilyushin, Ab Initio Study of the Formation of Vacancy and Hydrogen–Vacancy Complexes in Palladium and Its Hydride, Journal of Experimental and Theoretical Physics, **118** (2014) 80–86.

[33] Daisuke Kyoi, Toyoto Sato, Ewa Rönnebro, Yasufumi Tsuji, Naoyuki Kitamura, Atsushi Ueda, Mikio Ito, Shigeru Katsuyama, Shigeta Hara, Dag Noréus, Tetsuo Sakai, A novel magnesium–vanadium hydride synthesized by a gigapascal-high-pressure technique, J. Alloys Compd., **375** (2004) 253–258.

[34] S. Tavares, S. Miraglia, D. Frucharta, D.Dos Santos, L. Ortega and A. Lacoste, Evidence for a superstructure in hydrogen-implanted palladium, J. Alloys Compd., **372** (2004) L6–L8.

[35] H. Araki, M. Nakamura, S. Harada, T. Obata, N. Mikhin, V. Syvokon, M. Kubota, Phase Diagram of Hydrogen in Palladium, J. Low Temp. Phys., **134** (2004) 1145–1151.

[36] Y. Fukai, *The Metal–Hydrogen System*, Second edition, Springer-Verlag, (2005).

[37] O. Blaschko, Structural features occurring in PdDx within the 50 K anomaly region, J. Less-Comm. Met., **100** (1984) 307–320

[38] Atsushi Yabuuchi, Teruo Kihara, Daichi Kubo, Masataka Mizuno, Hideki Araki, Takashi Onishi and Yasuharu Shirai, Effect of Hydrogen on Vacancy Formation in Sputtered Cu Films Studied by Positron Annihilation Spectroscopy, Jpn.J.Appl.Phys., **52** (2013) 046501.

[39] Y. Fukai, The structure and phase diagram of M–H systems at high chemical potentials—High pressure and electrochemical synthesis, J. Alloys Compd., **404–406** (2005) 7–15.

Table 1: Sputtering conditions of the solid state electrolyte depositions.

Maker	Kyodo International Inc.
Target(s)	$BaZr_{0.8}Y_{0.2}O_3$ bulk ceramic (Toshima Manufacturing Co.,Ltd)
Machine	SRV4320 (Shinko Seiki Co.,Ltd)
Gas	Ar 48 sccm Ar + O_2 10% 2 sccm
Pressure	0.67 Pa
RF power	200 W
Substrate temperature	300°C
Deposition rate	1.75 nm/min

Table 2: Equivalent hydrogen pressures at the cathode by input voltage at 300°C. The hydrogen partial pressure in the chamber is assumed to be 0.013 MPa.

Input voltage	Hydrogen pressure (GPa)
0.5 V	3.22
1.0 V	15.9
2.0 V	56.3

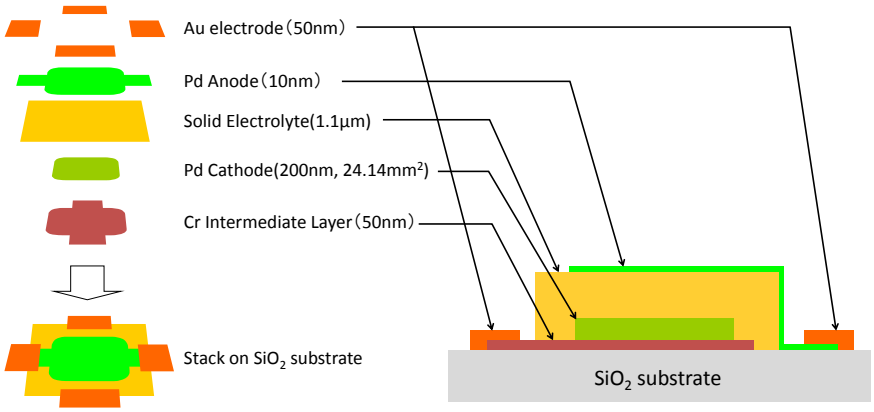

Figure 1: Stack structure of the electrolysis reactor. $BaZr_{1-x}Y_xO_3$ was employed for the solid state electrolyte. All layers were deposited on a SiO_2 substrate by sputtering using SUS metal masks. The solid state electrolyte layer was deposited at a substrate temperature of 300°C. Other layers were deposited at room temperature. Each anode and cathode has two electrodes for redundancy.

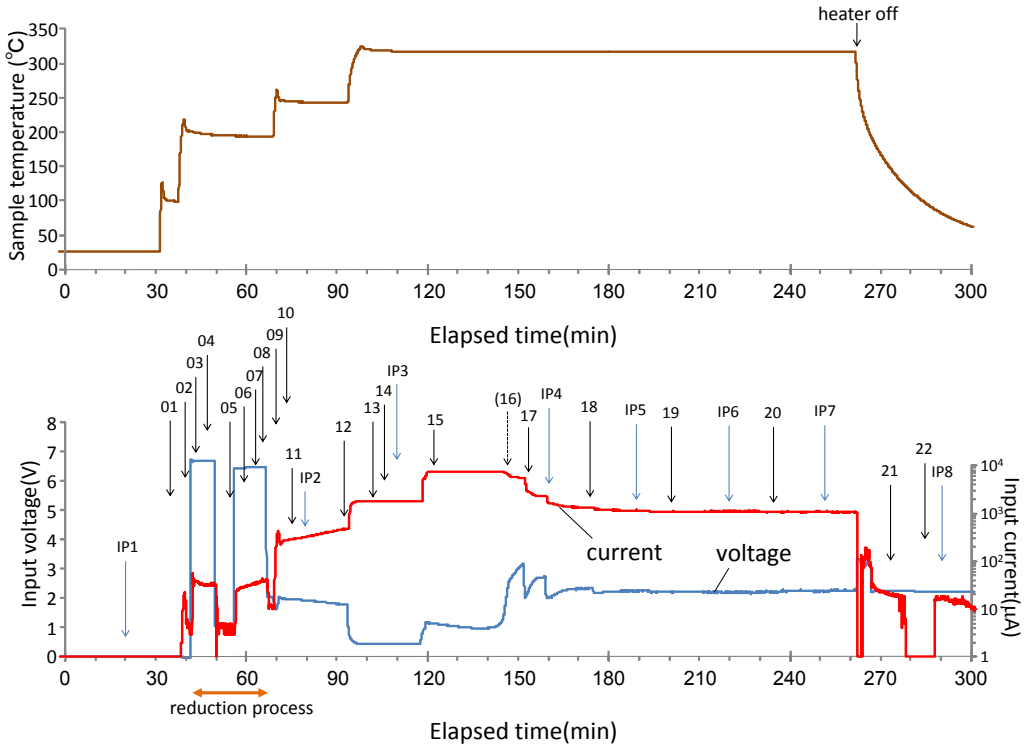

Figure 2: Testing temperature, input voltage, and input current as a function of time in the experiment. The initial 6 V input is the reduction process to reinforce adhesion of the electrolyte to the Pd cathode. Numbers with arrows denote the IDs of the timings of XRD measurements using a Pilatus pixel detector or imaging plate (numbers with "IP"). The numbers are referred to in Figures 3 and 4. The interruption between 50 and 57 minutes was caused by a mechanical fault of the synchrotron. Exposure No. 16 of the pixel detector at 147 minutes was unsuccessful.

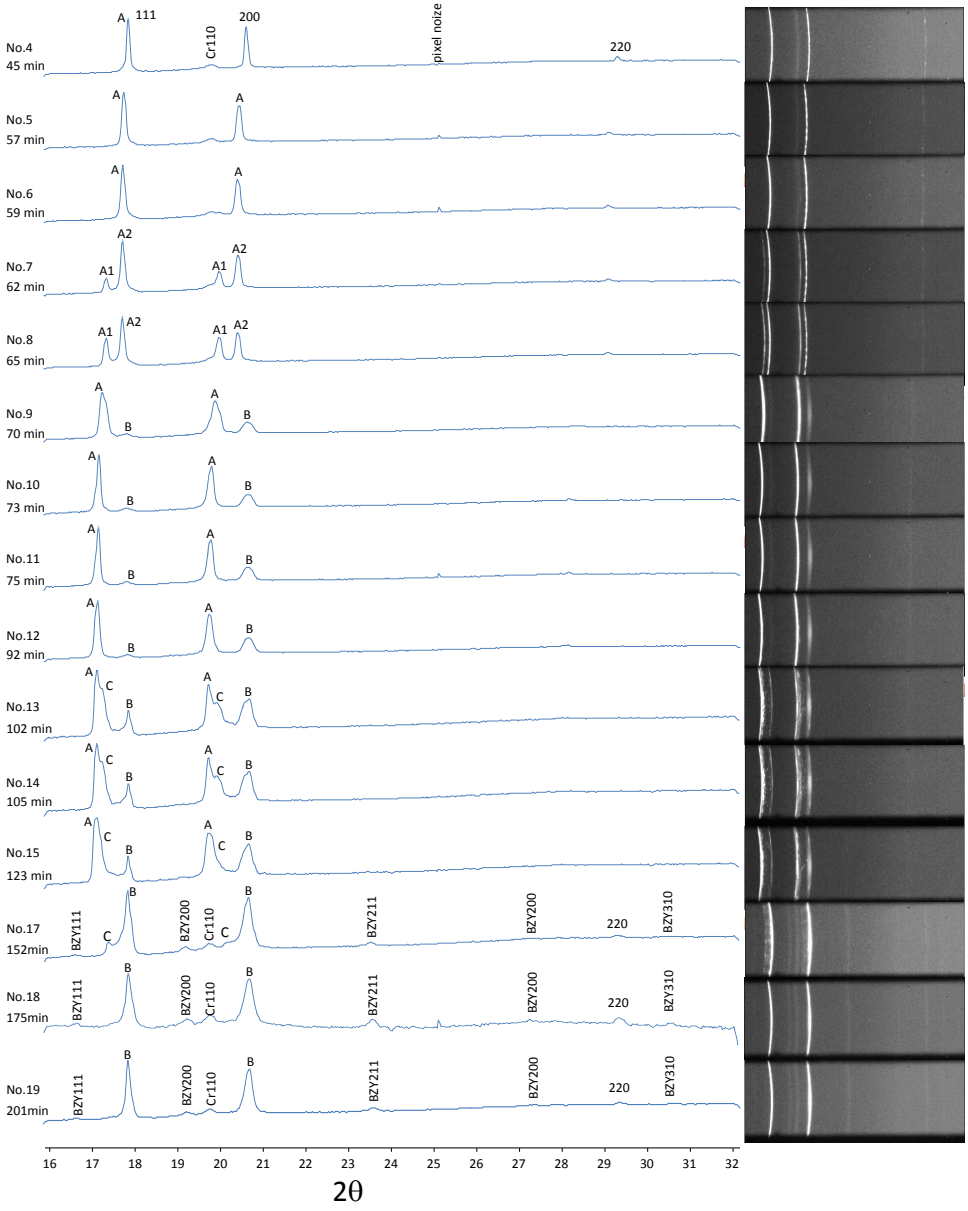

Figure 3: Diffraction images of the Pd cathode obtained by the Pilatus pixel detector. A shift in the diffraction line due to lattice expansion can be seen in Nos. 4 to 6 followed by phase separation into *A1* and *A2* at No. 7 and No. 8. Phase *B* appears from No. 9. Phase *C* appears from No. 13. Lines from the electrolyte (indicated as "BZY111") appear from No. 17. Phases *A*, *B*, and *C* are the vacancy-poor phase, vacancy-rich phase, and moderate-vacancy-concentration phase, respectively. The images were individually processed for optimized contrast, brightness, and noise-reduction. The numbers correspond to the IDs in Figure 2.

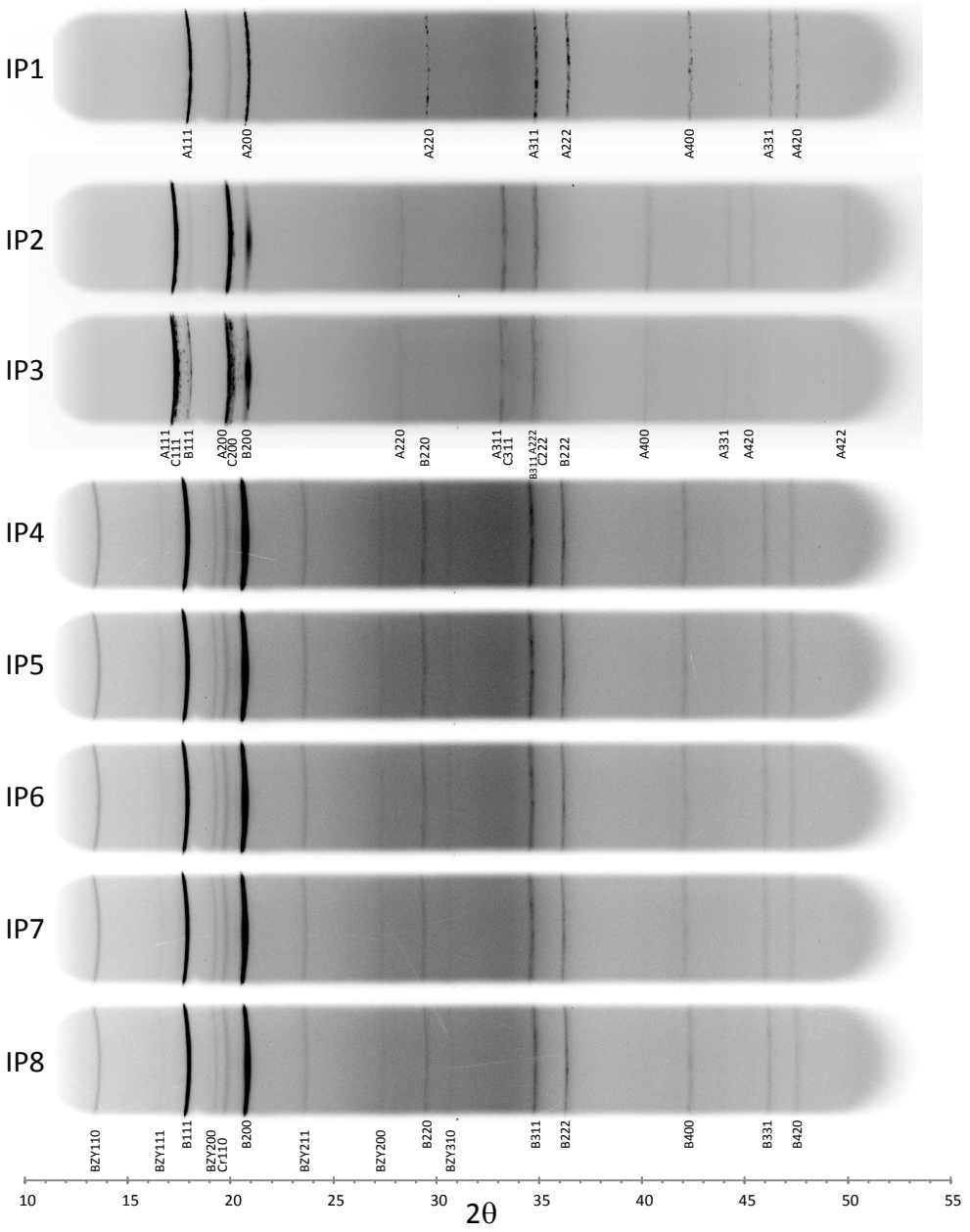

Figure 4: Diffraction images of the Pd cathode in the experiment obtained using the imaging plate. The IP2 and IP3, and IP4 to IP8 images were taken with multiple exposures on a single imaging plate.

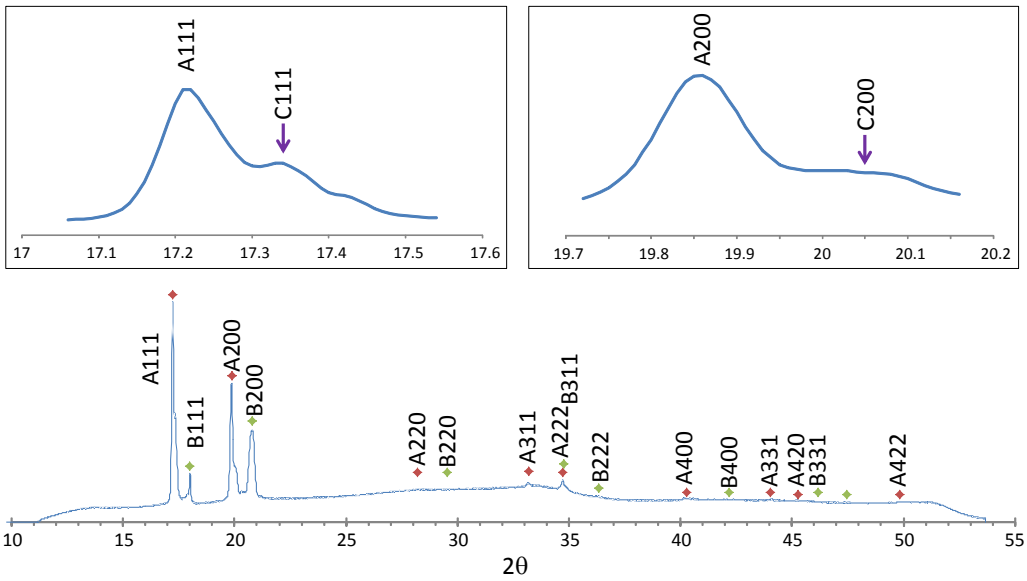

Figure 5: Diffraction spectrum of the Pd cathode in the experiment obtained at the third exposure of the imaging plate (IP3—110 minutes). The indicated reflection indexes are all for Pd. Phase C (moderate-vacancy-concentration phase) can be recognized as small sub-peaks near phase A (vacancy-poor phase). The insets show magnified diffraction spectra for 111 and 200.

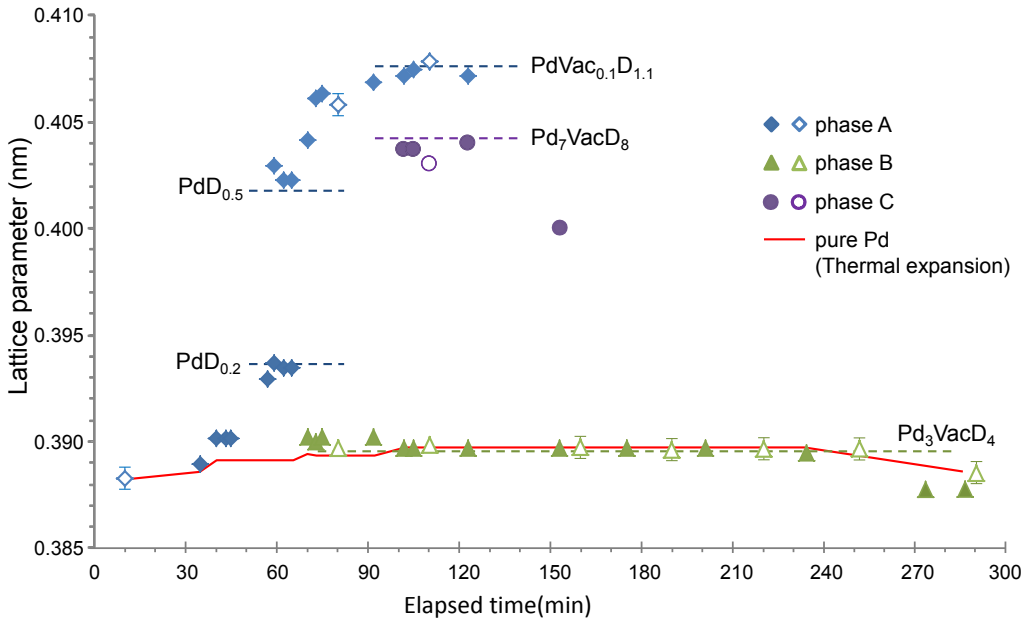

Figure 6: Lattice parameter changes in the experiment and comparisons with various types of Pd-hydrides containing vacancies. The filled plots were obtained by the Pilatus pixel detector. The open plots were obtained by the imaging plate. Error bars are shown for cases in which more than five diffraction lines were clearly identified. The red line indicates the calculated thermal expansion for pure Pd. 12μ/K of thermal expansion rate is assumed.

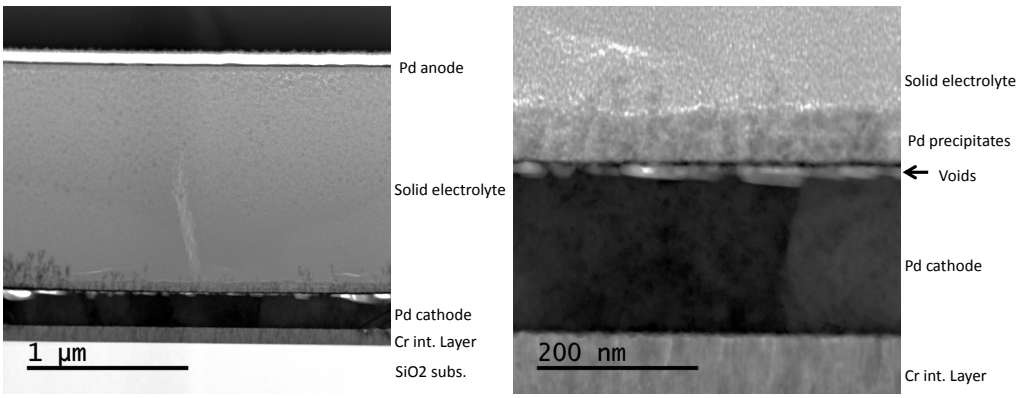

Figure 7: STEM images of the Pd cathode after the experiment.

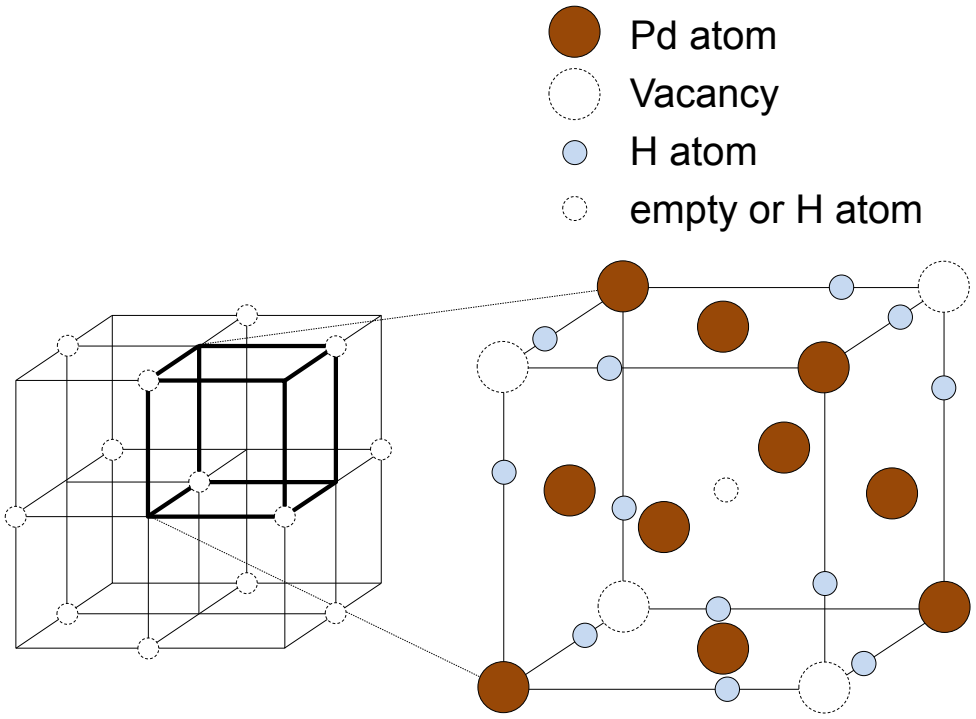

Figure 8: Possible super-lattice structure of $Pd_7VacH_{6\sim8}$. Left: super-cell structure, only vacancies are shown. Right: single-cell image, magnified from the part of the left diagram shown with bold lines. The hydrogen isotope atom at the body-centre does not bind to any vacancy. Therefore, the suffix-number of hydrogen varies within a range from six to eight.

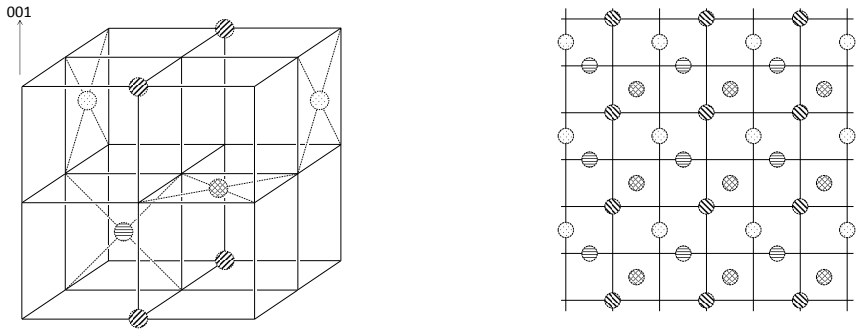

(a) (b)

Figure 9: Another possible super-lattice structure of $Pd_7VacH_{6\sim8}$. (a): super-cell structure. Only vacancies are shown. (b): lattice pattern along the (001) plane. Fill patterns show z-wise positions corresponding to the left diagram. All relative positioning between nearest vacancies are third-neighbour O-sites.